



Projected elevation-dependent warming in the Alps depicted with surface energy balance trends

5 Authors : Ian Castellanos¹, Martin Ménégoz¹, Juliette Blanchet¹, Julien Beaumet², Hubert Gallée¹, Eduardo Moreno-Chamorro^{3,4}, Chantal Staquet⁵, Xavier Fettweis⁶

¹Institut des Géosciences de l'Environnement, Grenoble, France

²Atmo Auvergne-Rhône-Alpes, France

³Barcelona Supercomputing Center (BSC), Barcelona, Spain

10 ⁴Now at: Max Planck Institute for Meteorology, Hamburg, Germany

⁵Laboratoire des Écoulements Géophysiques et Industriels, Grenoble, France

⁶Department of Geography, University of Liege, Liege, Belgium

Correspondence to: Ian Castellanos (ian.castellanos-dupuy@univ-grenoble-alpes.fr)

15

Abstract

Because of topography, climate change exhibits complex regional imprints in the Alps. This study aims at understanding the processes that link elevation-dependent warming (EDW) at seasonal scale in the Alps to the surface energy balance. We investigate projected EDW
20 patterns in the Alps using 7-km resolution simulations spanning the period 1961-2100 made with the Modèle Atmosphérique Régional (MAR), exploring scenarios SSP2-4.5 and SSP5-8.5 and driven by two general circulation models, EC-Earth3 and MPI-ESM1-2-HR. We find a larger yearly warming signal at high elevations (1.2 to 1.5 °C/°C of global warming) than at low elevations (1.1 to 1.3 °C/°C of global warming), with contrasted seasonal patterns and
25 intensities (up to 2 °C/°C of global warming at high elevations in summer). EDW signals are found to be different near the surface than in the free atmosphere, with a maximum signal in the former that is migrating to higher elevations through the seasons, linked to the snowline migration. Investigating surface energy balance trends reveals a link between the profiles of EDW and those of net shortwave radiation and energy used to melt snow. The snow-albedo
30 feedback linked to the net shortwave radiation trend is found to be responsible for two thirds of the impact of the snowline on warming, while snow melt accounts for the last third. Melting limits the warming at high elevation when snow is persisting. We suggest that snow melting is an important driver of EDW that should be considered in any EDW-snow investigations.

35



1- Introduction

Mountain regions are hotspots of biodiversity thanks to their often unique ecosystems which are vulnerable to rapid climate change (Rahbek et al., 2019). They host large water resources for both local and remote inhabitants (Viviroli et al., 2020), in relation to both orographic precipitation and snow and glacier melting, which can make downstream inhabitants eventually vulnerable to climate changes further up the slopes (e.g. Colombo et al., 2023). Their orography influences the atmospheric circulation at the synoptic scale, through local variation of the atmospheric flow and at the hemispheric scale through planetary waves triggered by the mountains, extending their influence to the surrounding regions.

Climate change in the mountains shows specific features, in particular because of potential Elevation-dependent warming (EDW). EDW is defined as the modulation with elevation of near-surface atmospheric temperature trends, a warming “along the slopes”. Although it is sometimes simplified as a linear regression of warming against elevation (e.g. Rangwala et al., 2010 ; Tudoroiu et al., 2016 ; Palazzi et al., 2017 ; Palazzi et al., 2019 ; Toledo et al., 2022), studies increasingly show nonlinearity in the dependency of warming with elevation (e.g. Kotlarski et al., 2012, 2015, 2023 ; Palazzi et al., 2017 ; Minder et al., 2018 ; Beaumet et al., 2021 ; Toledo et al., 2022 ; Napoli et al., 2023). Indeed, the drivers of EDW are numerous, interconnected, and may be confined to certain elevations. Hence, EDW signals are highly variable depending on the area and the period considered (Ohmura, 2012, Pepin et al., 2025). Pepin et al. (2015) give an overview of different processes that may impact EDW (albedo, clouds, water vapour, blackbody emission and aerosols) and the shape of their expected elevational dependency. EDW has been investigated in different mountainous areas : in the Alps (see reviews by Gobiet et al., 2014 ; Kuhn et al., 2020) ; in High Mountain Asia, small EDW signals have been reported over the last decades (Li et al., 2020) but these are expected to arise in future projections (Dimri et al., 2019). Contrasted EDWs are suggested for minimum and maximum daily temperature in the Andes, in relation with shortwave and longwave radiation changes (Toledo et al., 2022). In places where it has a strong seasonal cycle, snow is identified as one of the major drivers of EDW through the snow-albedo feedback (Rangwala et al., 2010 ; Kotlarski et al., 2015, 2023 ; Minder et al., 2018 ; Palazzi et al., 2019 ; Warscher et al., 2019 ; Beaumet et al., 2021 ; Byrne et al., 2024).

The Greater Alpine Region (GAR) is one of the most studied mountain regions in the world. Observation data broadly points towards an enhanced warming at high elevations in this region (Pepin et al., 2022), but an opposite signal can be found depending on the area and the period of interest (Philipona, 2012 ; Tudoroiu et al., 2016 ; Rottler et al., 2019). Overall, EDW in the GAR is not yet fully characterized and understood. This is mainly due to limitations in the amount of high-elevation observations on the one hand, and model grid resolutions that are coarse with respect to the orography on the other hand.

Simulations made with General Circulation Models (GCMs) are able to reach finer and finer resolutions as computational resources increase, but are still falling short of adequately



representing the complex topography in mountain regions (Sandu et al., 2019) and in the Alps in particular when studying climate change and its drivers (Palazzi et al., 2019). The need arises then to downscale these products to more suitable resolutions. Regional Climate Models (RCMs) are a frequently-used method to dynamically downscale GCMs. They allow
85 for simulations at ~10-km scale resolution or less, ensuring a better representation of the topography and the mountain climate.

As mentioned earlier, snow is a crucial driver of EDW, making it an important variable to represent correctly in simulations used to study climate change in mountain regions. A finer
90 model resolution improves the representation of snow (Lüthi et al., 2019), but even the 12-km resolution of the EURO-CORDEX experiments yields significant biases (Terzago et al., 2017 ; Matiu et al., 2020), highlighting the need for even finer resolutions. Most RCMs also have a simple representation of the snowpack, using a single layer varying in thickness over time. In our study, we use 7 km resolution experiments made with the Modèle
95 Atmosphérique Régional (MAR, Gallée and Schayes, 1994), a RCM further described in the next section, that uses a comprehensive multi-layer snow cover scheme.

MAR simulations at 7 km forced by the ERA-20C reanalysis have been performed previously to investigate the past evolution of climate and EDW in the Alps (Beaumont et al., 2021). The
100 results highlight seasonal contrasts in EDW over the period 1959-2010, with larger warming at low elevations in winter (< 1000 m.a.s.l.), at high elevations in summer (> 2000 m.a.s.l.) and at intermediate elevations in spring (1500-1800 m.a.s.l.). In this study, we aim to investigate the simulated EDW in the Alps under a stronger climate change signal associated with scenarios SSP2-4.5 and SSP5-8.5 from 1961 to 2100. In order to investigate
105 the processes driving EDW, we focus on the surface energy balance and the trends of its components. To our knowledge, this is the first study where all these components are analysed, in addition to using 140-years-long simulations until the end of the century at a high resolution.

110 First, the data and methods are described in Sect. 2. We delve into the results in Sect. 3 by : (i) exploring the warming footprints in the Alps in our simulations ; (ii) comparing EDW from near the surface to the free atmosphere ; (iii) investigating trends in the surface energy balance components and (iv) determining the evolution of the snowline and of the maximum trends for relevant variables. A discussion and a conclusion are offered in Sect. 4.

115

2- Data and methods

2.1 Model data

2.1.1 The Modèle Atmosphérique Régional (MAR)

120

MAR is a hydrostatic, primitive equation, limited-area model with constant sigma coordinates on the vertical axis (Gallée and Schayes, 1994 ; Gallée et al., 2005). It has been developed



125 for polar regions (e.g. Fettweis et al., 2017, Agosta et al., 2019, Amory et al., 2020) and
mountainous environments (e.g. Ménégos et al., 2013 over the Himalayas ; Ménégos et al.,
2020 and Beaumet et al., 2021 over the Alps ; Collao 2018 in Patagonia ; Fettweis et al.,
2023 in the Vosges mountain region), taking advantage of its comprehensive multi-layer
snow cover scheme (Brun et al., 1992). It has also been used over western Africa (Kouassi
et al., 2010, Chagnaud et al., 2020) to study the tropical hydrological cycle.

130 In the present work, data from simulations using two successive versions of MAR, 3.10 and
3.14, are analysed. Simulations made with version 3.10 were indeed missing some of the
surface energy balance components as diagnostic variables (see Table 1). A new simulation
using the latest version of MAR, version 3.14, was thus run in which all the variables of
interest were saved. Using both versions' simulations allows us to increase the spread of
135 investigated scenarios and climate sensitivities that we explore.

MAR version 3.10 uses a radiative transfer scheme developed by Morcrette (1991, 2002)
and used in the ERA-40 reanalyses (Uppala et al., 2005). Owing to some identified issues
within MAR of this scheme with downward radiation (e.g. Delhasse et al., 2020), and its lack
of modularity, the Morcrette scheme has been replaced by the ecRad radiation scheme
140 (Hogan and Bozzo, 2018) in version 3.14 of MAR (J.-F. Grailet, 2023). The second
difference between the two versions of MAR for the present paper lies in the climatology of
aerosols.

In version 3.10 aerosols have a yearly climatology that evolves until 2005 - later years use
the 2005 climatology. Version 3.14 by contrast uses the climatology provided by the
145 European Center for Medium Range Weather Forecasts (ECMWF, cycle 43r3 - see Bozzo et
al., 2020) which remains fixed throughout the whole simulation.

2.1.2 The simulations over the Alps

150 MAR is applied over the Alps at a 7 km resolution. This resolution was chosen to depict the
alpine topography - with its narrow valleys - more accurately than the 12 km EUROCORDEX
resolution while still being compatible with the hydrostatic approximation in middle latitudes
configurations (which imposes a ~5-10 km resolution at the lowest). This resolution
smoothes the Alps to a maximum elevation close to 3500 m.a.s.l. while the real maximum
155 elevation is 4808 m.a.s.l. at the Mont Blanc. The domain extends from 1.5 to 18.5° E and
from 41.5 to 49.5° N (Fig. 1).



5

Temperature (°C)	
T2m	Daily mean temperature at 2 meters above the surface
Tp	Daily mean temperature at different pressure levels
Tmin	Minimum daily temperature at the first atmosphere layer (sigma level)
Tmax	Maximum daily temperature at the first atmosphere layer (sigma level)
ST	Daily mean surface temperature
Surface energy balance, daily mean (W/m²)	
NSW	Net shortwave radiation (difference between downward and upward flux)
NLW	Net longwave radiation (difference between downward and upward flux)
LHF	Latent heat flux
SHF	Sensible heat flux
Melt top*	Snowmelt energy flux at the topmost layer
Freeze top*	Freeze energy flux at the topmost layer
GF*	Ground flux
HAcc*	Heat accumulation in the topmost layer
SWt*	Shortwave radiation transmitted to lower layers (only with snow, as soil layers are opaque in the model)

Table 1 : MAR variables used in this study. Variables with a * are only available for the MAR version 3.14 simulation.

160

From the CMIP6 database (Eyring et al., 2016), we retained for our study the two GCMs showing the best skill over the European-North-Atlantic area (80° W-45° E, 35° N-75° N) : EC-Earth3 and MPI-ESM1-2-HR. This choice is based on a comparison with the ERA5 reanalysis over 1971-2000, using the weighted mean square error of 3 variables : the temperature at 700 hPa, the geopotential height at 500 hPa, and the surface ocean temperature weighted at half weight. These variables were selected to evaluate the skill of the GCMs to reproduce large-scale circulation (and ocean-atmosphere interactions), as the RCM is expected to represent the smaller scale processes. The selected criteria and forcing GCMs are consistent with the recommendations detailed in Sobolowski et al., 2025. CMIP6 simulations include a historical period available over 1850-2014 and future projections over 2015-2100, based on different scenarios, including in particular the intermediate greenhouse gas emissions (SSP2-4.5) and the high emission scenario SSP5-8.5 (O'Neill et al., 2016).

175 In this study, we use the following four 1961-2100 simulations made with either version 3.10 or version 3.14 of MAR :



- MAR version 3.10 forced by EC-Earth3 (historical, 1961-2014 ; SSP2-4.5, 2015-2100) ;
- 180 - MAR version 3.10 forced by MPI-ESM1-2-HR (historical, 1961-2014 ; SSP2-4.5, 2015-2100 ; SSP5-8.5, 2015-2100) ;
- MAR version 3.14 forced by MPI-ESM1-2-HR (historical, 1961-2014 ; SSP5-8.5, 2015-2100).

Hereafter, the simulations will be referred to as MAR-EC-Earth3 SSP2, MAR-MPI SSP2,
185 MAR-MPI SSP5, and MARv3.14-MPI SSP5 respectively.
The v3.10 MPI simulations have previously been presented in Bacer et al. (2024). We
include here the v3.10 MAR-EC-Earth3 SSP2 and MARv3.14-MPI SSP5 simulations.

We present the variables (and associated acronyms) used in this study in Table 1.
190 The outputs of MAR are described in Appendix A, along with the surface energy balance in
the soil and snow routine in MAR.
A data set for a limited number of variables and levels is available online (see “Data
availability” at the end of this paper).

195 Beaumet et al. (2021) find biases in temperature and snow cover in the Alps in MAR
simulations forced by reanalyses (ERA-20C and ERA5) when comparing to gridded
observational datasets, reanalyses and in-situ observations. In their study, the MAR
experiments are found to slightly overestimate temperature at low elevations and
underestimate at high elevations, especially in winter. They also are found to underestimate
200 snow cover duration at low elevation (< 1500 m.a.s.l.). Nevertheless, the biases found are
typical of RCMs and are overall considered acceptable.
By comparing the MAR simulations used in the present study to gridded observational
datasets based on station interpolation (see Appendix B), these simulations were found to
have a cold bias reaching maximum values up to 3 °C at high elevations (above ~2000
205 m.a.s.l.) across the seasons and a generally warm bias at lower elevations (below 1000-
1500 m.a.s.l. depending on the season), especially in summer for which it can reach
maximum values of 4 °C. There is also a wet bias in precipitation at high elevation (above
1500 m.a.s.l., except in summer which has a dry bias) reaching around 7 mm per day in
winter. Lower elevations (below ~1000 m.a.s.l.) tend to have a dry bias (~2 mm on average,
210 up to 5 mm) in summer and autumn. Also, compared to satellite estimates (Appendix B),
MAR shows a too long snow cover duration at high elevations (above ~2000 m.a.s.l.) for all
seasons (a bias reaching maximum values of 50 additional days of snow in spring and
summer), and a too small amount of snow days at low elevations (below ~1000 m.a.s.l.) in
winter (up to 40 fewer days of snow). The biases provided here are an estimation, since
215 observational datasets over the Alps also have large uncertainties, due in particular to the
inherent missing values in such products (Prein and Gobiet, 2017 ; Kotlarski et al., 2019 ;
Matiu et al., 2024) that are not discussed in this article.

220

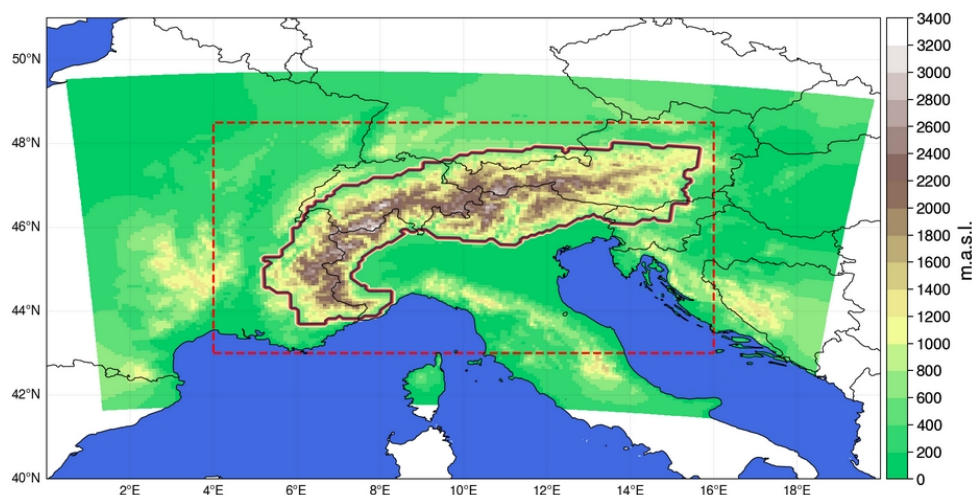


Figure 1 : Domain and topography of MAR simulations. The contour defines the Alps (see Sect. 2.2.2) and is used as a mask further on in this paper (e.g. whenever there is a value averaged over the Alps). The red box is the area shown in Fig. 2, corresponding to the domain considered after excluding the lateral parts affected by boundary conditions in the MAR experiments.

2.2 Methods

2.2.1 MAR warming as a function of global warming

As a preliminary step before studying EDW, we produce the maps of MAR warming as a function of global warming. For this, we combine all three v3.10 simulations (excluding the v3.14 simulation to avoid giving too much weight to the same model-scenario pair).

We first compute the global warming in each GCM forcing simulation by averaging yearly as well as spatially the global monthly 2-meter air temperature from 1850 to 2100. We then fit a 3rd degree B-spline using 4 knots through the resulting series of 251 yearly global temperature. This allows us to have a smooth correspondence between any given year and the global mean temperature in the forcing simulation (see Appendix C). We choose 1961-1990 as a reference period to compute the warming anomaly (subtracting the mean of the reference period to the global mean temperature spline). We regress at each gridpoint the three merged MAR v3.10 anomalies onto the global warming level given by the splines. This allows us to get an estimation of the local warming as a function of global warming. Finally, we apply the same procedure at the seasonal scales.



2.2.2 Altitudinal trends in the Alps

In this study, we consider historical and projected trends for temperature and surface energy balance fluxes. The historical period spans 1961-2014 and the projection 2015-2100. For each grid point, period and variable of Table 1, we compute the trend in the seasonal mean with a linear regression against the years.

In order to consider altitudinal trends at the scale of the Alps, we first apply a mask to our data to isolate the Alps, by selecting the grid points that satisfy the two conditions of being at least 360 meters above sea level (m.a.s.l.) and having a neighbouring grid point at 1300 m.a.s.l. or more (see the contours in Figures 1 and 2).

Then, we classify the grid points into 200 m-altitude bins and compute the mean and standard deviation of the trends for each bin, for any given variable. The temperature in the free atmosphere is the only variable that is not classified in bins, as it is available at seven different pressure levels in the MAR v3.10 outputs (five in version 3.14).

2.2.3 Elevation change of maximum trends

In order to track the evolution of the elevation of the maximum trend (defined below) in temperature and surface energy balance fluxes, we first smooth the seasonal data at each grid point by fitting a 3rd degree spline with the year as covariate (implemented with an adaptive smoothing parameter s used to choose the number of knots, $s = N \cdot v$ with N the number of years and v the variance of the yearly series), in order to remove the year-to-year noise. Then, we divide the 1961-2100 simulation into 90 overlapping 50-year windows (1961-2010, 1962-2011, ..., 2051-2100) and compute the difference between the first and last year of the estimated spline at each grid point and for each window. At this point we have one trend per grid point and window.

Then, for each window, we fit another 3rd degree B-spline using 5 knots through the scatter plot of grid point trends versus the elevation. We take the elevation of the maximum warming after excluding the lowest 10 % and highest 0.3 % elevations of the spline to properly target the local maximum at intermediate elevations in windows that feature a global maximum at the bottom or the top of the altitudinal range (see Appendix D). For each variable, we end up with an elevation of maximum trend for each window, and thus with a temporal evolution of the elevation of maximum trend.

2.2.4 Snowline elevation

The snowline elevation can be computed with different methods, and three of them are provided here : We compute over the Alps and for each day (i) the mean elevation of the 10 highest grid points having < 1 millimeter water-equivalent (mmWe) of snow, (ii) the mean elevation of the 10 lowest grid points having ≥ 1 mmWe of snow, and finally (iii) the average of these two criteria. The first criteria gives an estimate of the elevation above which all grid points have snow, the second criteria the elevation below which no grid points have

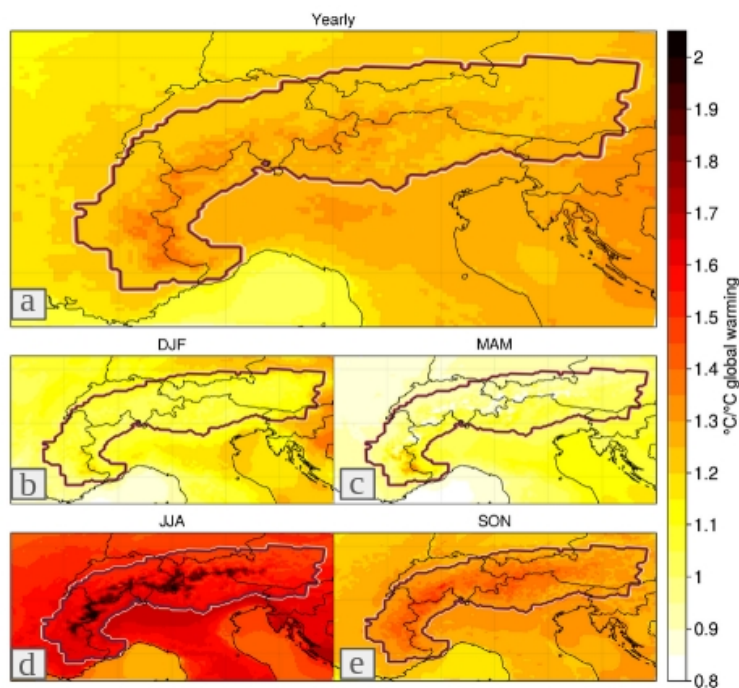


snow. The two elevations define a snow transition band between them, in which some grid points have snow and some don't.

290 We then take the seasonal median of these daily values to get an average of the snow line elevation over the whole period or window.

3- Results

3.1 Warming footprint in the Alps



295 Figure 2 : (a) Yearly warming in the three v3.10 simulations scaled with respect to global warming level in the forcing GCM. (b), (c), (d), (e) : same as (a) at the seasonal timescale. See Figure 1 for the definition of the contour line.

300 Figure 2 shows the yearly and seasonal warmings in the three v3.10 MAR simulations with respect to global warming (see Sect. 2.2.1). As seen in Fig. 2a, yearly temperatures are rising faster at higher elevations in the Alps (~1.2 to 1.5 °C/°C) than in the surrounding lowlands, which are already warming at a faster rate than global warming (~1.1 to 1.3 °C/°C). There is also a strong longitudinal gradient in this area, the continental climate in the
305 Eastern part warming faster than the Western European climate that is under an oceanic influence.



10

Overall, strong seasonal contrasts can be seen both in warming intensity and pattern over the Alps (Figs. 2b, c, d, e).

310

The warming is particularly intense in summer (JJA) with values around 1.6 to 1.7 °C/°C global warming in the lowlands, and reaching twice the global warming at high elevations. In contrast, the domain warms at a similar rate to global warming (1-1.1 °C/°C) in spring (MAM) and at even lower rates (0.8-0.9 °C/°C) at high elevation, except in the southern Alps.

315

Autumn (SON) is similar but less extreme than summer, while winter (DJF) is similar to spring, albeit showing a slightly higher warming rate.

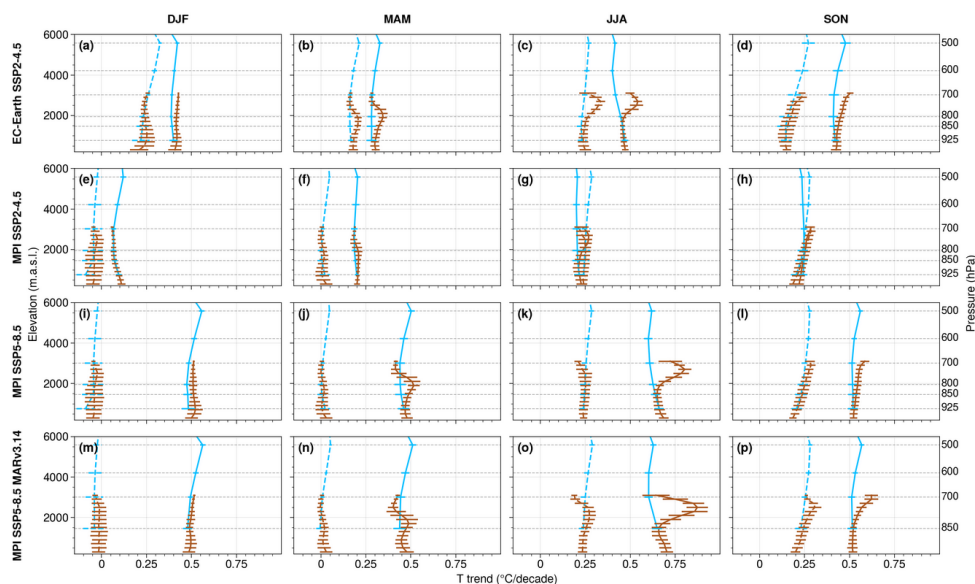
The pattern of warming is opposite between summer and spring : summer shows its highest rates of warming at high elevations, where spring shows its lowest rates of warming. The exception being in the southern Alps, where this pattern is reversed.

320

It is therefore essential to consider seasonal timescales in order to understand the processes that are behind these contrasting patterns.

3.2 Elevation-dependent warming near the surface and in the free atmosphere

325



330

Figure 3 : Alpine temperature trends near the surface (along the slopes) averaged over 200 m-altitude bins (T2m, brown) and in the free atmosphere averaged over the available pressure levels (Tp, blue). The historical period (1961-2014) is in dashed lines, projection (2015-2100) is in full lines. Horizontal bars are the spatial standard deviation (1 sigma). The first three rows are the MAR v3.10 simulations. Columns are for each season.



335 Figure 3 shows the temperature trend 2 meters above the surface and in the free
atmosphere (at different pressure levels) at the scale of the Alps, for the four simulations
over the historical (1961-2014) and the projection (2015-2100) periods, using the method of
Sect. 2.2.2.

340 Overall, the warming is generally larger in the projection than in the historical period, both in
the free atmosphere and near the surface. The exception is in summer and autumn for the
MAR-MPI SSP2 simulation (Figs. 3g and 3h) where the two periods experience similar
warming. The lowest temperature trend is close to zero in winter in the historical period for
the MPI simulations (Figs. 3e, 3i and 3m). The largest warming is simulated in summer with
345 the MARv3.14-MPI SSP5 simulation (Fig. 3o) and reaches 0.86 °C/decade on average at
2500 m.a.s.l., i.e. almost 7.4 °C of warming between 2015 and 2100.

Looking at their vertical profiles, the rates of warming in the free atmosphere and near the
surface have a similar altitudinal gradient in winter. The trend values are similar, with slightly
350 larger trends for the near-surface warming and a larger spatial standard deviation.
In spring, the same can be generally said for the low and high elevations. However, we can
see higher rates of warming at mid-elevations near the surface than in the free atmosphere
for both periods in MAR-EC-Earth3 SSP2 (Fig. 3b), and for the projection periods of MAR-
MPI SSP5 (Figs. 3j and 3n).

355 For MAR-EC-Earth3 SSP2, in spring, the maximum of warming near the surface is found at
a higher elevation in the projection than in the historical period, suggesting an upwards
migration of the underlying cause for this heightened near-surface warming.
In summer and autumn, the near surface maximum warming signal moves at higher
elevations, with the strongest signal seen in summer for MARv3.14-MPI SSP5 (Fig. 3o).

360 This enhanced surface warming appearing at mid-elevations in spring, moving upwards and
increasing in summer, and continuing to move upwards with a lower intensity in autumn, is
investigated along with its link to surface processes in the next section.

365 In some simulations and periods, we also see a rate of warming lower near the surface than
in the free troposphere that is located above the elevation of the maximum warming. This
can particularly be seen in the SSP5 simulations in spring for the projection (Figs. 3j, 3n) and
in summer for the historical period (Figs. 3k, 3o).

370 In the free atmosphere, the warming is generally more skewed towards lower (925hPa) and
higher (500hPa) elevations in the projection period than in the historical period (see panels
a, c, d, e, i, j, k, l, m, o, p of Fig. 3). This leads to some altitudinal trends having a hook
shape, further discussed below (see Sect. 4). The warming in the free atmosphere in the
MAR experiment is following very closely the warming simulated in the forcing GCMs,
375 especially at high elevations (not shown). This highlights low atmosphere and surface
feedbacks simulated with MAR that cannot be solved by the GCMs whereas the regional
climate is driven by large-scale features of the GCM projections.

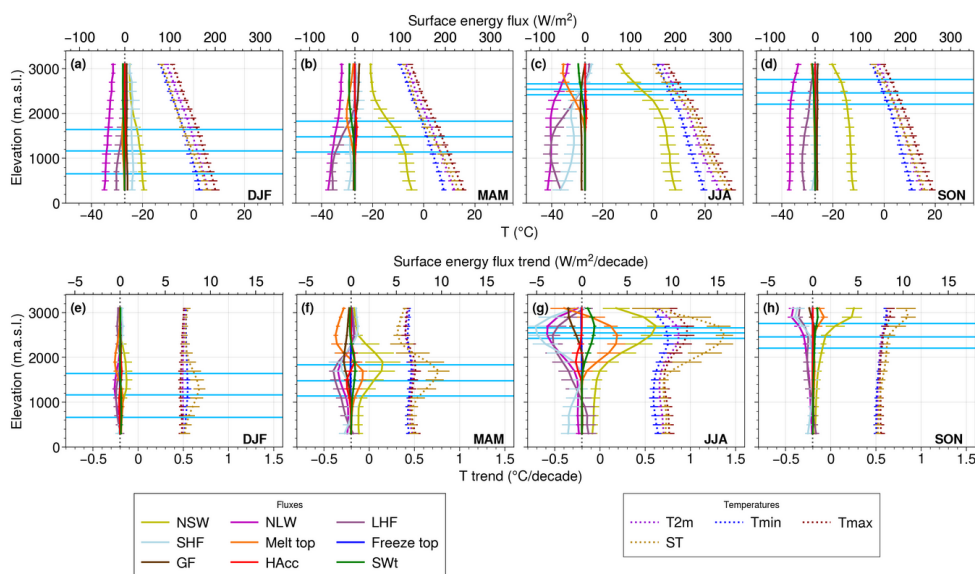
380 In the continuation of this study, we investigate this seasonal signal occurring near the
surface by analysing the surface energy balance fluxes and their respective trends.



3.3 Projected temperature and energy flux trends

We define the surface energy balance in the model MAR as the sum of all fluxes occurring at the first surface layer of the ground and of the processes occurring within that layer - heat accumulation, snow melt and water refreezing. In this model, the first surface layer of the ground is 1-mm thick in the absence of snow and has the (variable) depth of the first snow layer in the presence of snow. The surface energy balance is expected to be closed, meaning that the sum of the fluxes is expected to be equal to zero. By identifying all the variables that are part of this balance (see Sect. 2.1) and computing their trends, we ensure that we have a comprehensive view of what is happening at the surface and that we do not overlook any process contributing to increased surface warming. Only MARv3.14 results are used here as this version allows to display all the different energy fluxes. The two versions have similar EDW trends in the Alps as displayed by the last two rows in Fig. 3.

395



400 Figure 4 : Altitudinal profiles of the projected (2015-2100) mean values (top) and trends
 (bottom) for temperatures (dotted) and fluxes (full lines) averaged over the Alps, in the MAR
 v3.14 simulation. For each panel, the temperature (trend) values are indicated on the lower
 axis and the surface energy flux (trend) values on the upper axis. Horizontal bars are the
 spatial dispersion (1 sigma). Blue horizontal lines refer to the altitude of the snowline
 405 computed in three different ways (cf. Methods/Sect. 2.2.4). Fluxes are positive when directed
 towards the surface. Season is indicated in the bottom right corner.

Figure 4 displays the altitudinal profiles of the projected mean values and trends for



410 temperatures and surface energy fluxes. The blue horizontal lines indicate the mean altitude
of the snowline for each season using the method presented in Sect. 2.2.4. The top and
bottom lines can be seen as a snow transition band including the snow line.

415 The average values (top row) highlight the sign and the vertical distribution of the
temperature and surface energy fluxes. Fluxes are defined as positive when directed
towards the surface. The mean NSW flux is positive for all seasons with a seasonal cycle
that reaches its maximum in summer, as expected, and decays with height. A stronger
decay above the snowline showcases the impact of the presence of snow on the NSW flux.
420 The mean NLW flux is the main component balancing the NSW flux, and as such has a
similar profile except that it is negative and follows a weaker seasonal cycle. The SWt flux is
negative in the presence of snow, since it is being transmitted to the lower layers from the
surface, and equal to zero in the absence of snow since the ground is opaque in the model.
The mean LHF is negative (except at the top), meaning that evaporation is cooling down the
surface (humidity transfer from the surface to the atmosphere). It decreases with height as
425 well - which might be due to less available NSW flux at high elevations - except at the
bottom in summer (Fig. 4c), which might be due to less available humidity at low elevations.
The mean SHF is positive in winter, indicating that the surface is being heated up by
turbulent fluxes in the surface boundary layer (ST is cooler than T2m). It is negative at low
elevations in spring, summer, and autumn, as ST is warmer than T2m, and switches sign at
430 higher elevations. Mean melt top is always negative by convention (energy is used by the
surface to melt snow) and largest in summer. It is larger at intermediate elevations in winter
and spring, because temperature is too low to induce melting at high elevation, and larger
near the top of the altitudinal profile in summer and autumn. We do not delve into the other
variables because of their low amplitude.

435 The bottom row of Fig. 4 shows that T2m, Tmin and Tmax exhibit similar trends, while ST
exhibits the largest trend, near the top of the snow band. This suggests again that the
maximum T2m trends are mainly driven by surface processes. The closer to the surface, the
stronger the temperature trend signal. The surface absorbs more energy over time which is
440 then redistributed to the near-surface atmosphere thanks to the longwave radiation and
sensible and latent heat fluxes, explaining the temperature signal found close to the surface
that shows a similar shape but with a smaller intensity.
In spring and summer, ST also exhibits a minimum trend at higher elevations.

445 Let us remember that a positive trend means an *increase* for a positive flux, but a *decrease*
for a negative flux. NSW and NLW fluxes both show a clear increase in their absolute values
over time and throughout the seasons, which is expected in a warming climate. By contrast,
SWt is decreasing, which is explained by the decrease in snow cover over time.
LHF and SHF have large trends that generally point to an absolute increase, but not for all
450 elevations, as both the mean values and the trends switch signs at different elevations and
seasons. They might be in part a response to the perturbations in NSW flux and melting.
GF, HAcc and Freeze have small or non-existent trends.

Melting flux shows large trends in spring and summer. For both seasons, the trend first
455 increases with elevation, then decreases until it ends as a negative trend near the top of the
elevational gradient. As seen with the temperature, the melt trend is larger and shifted to
higher altitudes in summer compared to spring, as expected. The presence of both a
maximum trend, and then a minimum trend at higher elevations, is reminiscent of the surface
temperature trend and the lower rate of warming above the maximum signal discussed in the
460 previous section.



Figure 4 shows evidence that the snow-albedo feedback is the main driver of the elevation-dependent warming signal. Indeed, the NSW variable shows the largest trend at the snow transition band elevations. The NLW, SHF and LHF trends compensate for this increase to maintain the surface energy balance with a maximum trend at similar elevations but negative in sign.

Melting strongly impacts the surface energy balance and temperature as well, with a positive trend within the snow transition band, transitioning to a negative trend above. The snow melt energy flux is negative (top row of Fig. 4) which means that the snow melt increase (negative trend) is slowing down the warming at elevations where there are still significant amounts of snow, and the snow melt decrease (positive trend) is speeding up the warming where snow is becoming scarce. This is due to the phase transition from solid to liquid water. When the snowpack reaches 0 °C, additional energy provided by e.g. solar radiation is consumed to melt the snow without an increase in temperature in the system. Once the snowpack is no longer present, the energy which was used to melt the snow is back to increasing the surface temperature once again.

In spring, the spatially averaged trend of the snow melt energy flux reaches a maximum of 1.31 W/m²/decade and a minimum of -1.71 W/m²/decade, while the spatially averaged NSW trend reaches a maximum of 3.50 W/m²/decade. If we subtract to these values the trend seen at low elevations to isolate the effect of the snowline, the NSW trend is closer to 2.63 W/m²/decade and the melt to 1.27 and -1.75 W/m²/decade.

In summer, the mean trend of the snowmelt energy flux reaches a maximum of 3.90 W/m²/decade and a minimum of -1.96 W/m²/decade, while the NSW trend reaches a maximum of 8.18 W/m²/decade. Subtracting the trend at low elevations to estimate the effect of the snowline alone, the NSW trend is closer to 7.12 W/m²/decade (melt is unchanged). For both seasons, the NSW maximum trend is slightly more than twice the snow melt energy flux trend (either positive or negative). This means that while the snow-albedo feedback effect is the main cause behind the simulated elevation-dependent warming in both seasons, the snow melt change is also having a significant effect on the warming at and near the surface.

The snowline is expected to migrate upwards with global warming. In the continuation of this study, we investigate if there is a similar migration in the elevations of the maximum trends.



15

3.4 Snowline and elevation of maximum warming

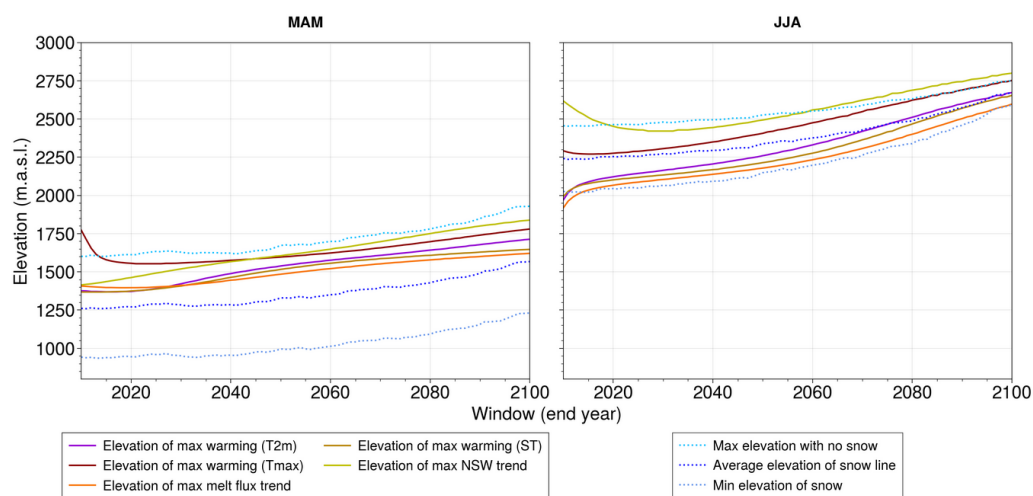


Figure 5 : Elevation of snowline, maximum warming trends (T2m, Tmax, ST), melt flux trend and net shortwave trend in spring and summer over the course of rolling 50-year windows spanning 1961-2100 in the MAR v3.14 simulation over the Alps. The final year of each window is shown on the x axis.

Figure 5 shows the evolution of the elevation of the maximum trend throughout the MARv3.14-MPI SSP5 simulation spanning 1961-2100 for T2m, ST, Tmax, NSW and the melt flux for rolling 50-year windows (see Sect. 2.2.3). Superimposed is the elevation of the snowline using the criteria defined in Sect. 2.2.4 for each 50-year window.

In spring, the snow transition band migrates by approximately 300 meters to higher elevations between the first (1961-2010) and the last (2051-2100) windows. The elevations of the maximum trends are contained within this band and shift similarly, with shifts ranging from 200 meters to over 400 meters (not counting the first few windows for Tmax where the maximum trend is higher than expected).

In summer, the snow transition band is narrowing and migrates to upper elevations. The top of the band increases in elevation by approximately 300 meters between the first and last windows, the bottom by approximately 550 meters. The elevations of the maximum trends are again mostly contained within this band. They migrate upwards by 450 to 650 meters, except for NSW which is unexpectedly high and decreasing in elevation for the first 10-15 windows.

This suggests a correlation between the migration of the snow transition band and the elevation of maximum warming, the latter staying largely contained within the former in spring and summer in the span of the entire simulation.



4 Discussion and conclusion

525

In this study, we analysed four MAR simulations over the Greater Alpine Region in order to investigate the physical drivers of EDW. We saw higher warming in the Alps compared to the global warming simulated in the forcing GCMs : 1.2 to 1.5 °C/°C at the yearly timescale. The warming reaches higher values in summer, with values around 1.7 °C/°C at low elevations and up to 2 °C/°C at the highest elevations. We found a reversed EDW in spring, with a warming at high elevation that reaches lower values than the global warming (0.8-0.9 °C/°C). The different warming patterns from season to season highlighted the need to investigate EDW at the seasonal timescale. Then, we compared the warming near the surface (along the slopes) and in the free atmosphere and highlighted a maximum signal along the slopes moving upwards from spring to summer to autumn. This local warming is explained by surface-atmosphere exchanges, since it does not happen in the free atmosphere. There is no clear EDW in winter, which could be explained by a lower available amount of solar radiation, making temperature trends less dependent on its variations at the surface. Among the different surface energy fluxes, NSW and melt energy fluxes have a maximum trend at a similar elevation than the maximum temperature trend, located near the top of the snow transition band (i.e. where the snow starts to disappear in a warming climate). Almost two thirds of this maximum warming is explained by NSW changes (2.63 W/m²/decade in spring, 7.12 W/m²/decade in summer), whereas melting changes contribute over a third in our model experiments (-1.75 to 1.27 W/m²/decade in spring, -1.96 to 3.90 W/m²/decade in summer). Finally, we saw that the trends of T2m, Tmax, ST, NSW and melting fluxes show a maximum value at an elevation that moves upward over time. This happens at the elevation of the snow transition band, i.e. in the elevation band covering the areas where the snow cover starts to disappear and where the last snow patches are remaining.

530

535

540

545

550 An added value of the simulations used in this study compared to previous studies on EDW in the Alps with model data (Kotlarski et al., 2012, 2015, 2023 ; Gobiet et al., 2014 ; Palazzi et al., 2019 ; Lüthi et al., 2019 ; Warscher et al., 2019 ; Beaumet et al., 2021 ; Napoli et al., 2023) is the combination of (i) a fine resolution at 7 km ; and (ii) a large timespan of 140 years covering both a historical and projection periods. The 7 km resolution allows for a good compromise between the representation of the alpine topography (to reduce snow cover biases seen e.g. at 12 km in the EURO-CORDEX experiments ; see Terzago et al., 2017, Matiu et al., 2020) and the hydrostatic approximation required in MAR experiments. The large timespan allows for investigating trends in a context where natural variability induces small signal-to-noise ratios.

555

560 Pepin and Seidel (2005) find enhanced warming at the surface compared to the free atmosphere in global mountain regions by comparing surface temperature in observation data sets and free atmosphere temperature from an interpolated reanalysis product for the period 1948-1998. However, the weakest signal in absolute value is found for locations over Europe (see Table 4 within). In the Rocky Mountains, Minder et al. (2018) find stronger warming rates along the slopes than in the free troposphere in RCM experiments, highlighting the role of the snow-albedo feedback. To our knowledge, our study is the first one that is providing a similar finding in the Alps, with a complete view of all the surface processes at play.

565



570 The melting of snow consumes energy due to the phase transition of snow to liquid water. This process limits the warming above the snowline at elevations where melt is increasing, and enhances the warming below the snowline where melt is decreasing. As stressed above, we find that it is responsible for approximately a third of the snowline's impact (positive or negative) on warming in the MAR version 3.14 simulation. We suggest that this process is a driver of EDW and should be considered in any EDW-snow investigations.

575 The impact of snow on elevation-dependent warming is often simplified to the snow-albedo feedback effect (e.g. Pepin et al. 2015, Palazzi et al., 2019, Warscher et al., 2019 ; Byrne et al., 2024). Thornton et al. (2021) identify snow melt as an essential mountain climate variable, but from a hydrological standpoint only. Dimri et al. (2022) investigate snow melt trend as a function of elevation in the Indian Himalayan region, seeing a similar signal to ours : the snow melt trend transitions from positive (the melting process decreases over time) to negative (that process increases) when going from low elevations to high elevations. The signs of the trends are reversed in their study as they look at the snow melt in kg/m^2 , which is positive, while the present study looks at the melt contribution to the surface energy balance, which is negative. However, they do not mention a possible contribution of the energy consumed by snow melt, again only mentioning the effect on albedo. Minder et al. (2018) find, when removing the snow-albedo feedback, similar EDW profiles between the free troposphere and near the surface. However a small signal near the surface remains in their study. We may hypothesize this to be the melt energy flux in light of our study.

580

585

590 Our study is based on a small ensemble experiment (two configurations with two different forcing GCMs, one of them with two scenarios). We use a single RCM, which has its own climate sensitivity (Glaude et al., 2024). Larger ensemble experiments would help to diagnose the temperature and snow changes, disentangling the forced signals versus those related to climate internal variability. Nevertheless, it is useful to identify the patterns and the physical drivers of EDW with single experiments, since ensemble averaged signals might overwhelm the local enhanced trends that might differ among GCM-RCM configurations.

595

Two main limitations appear in our model framework: (i) we are considering a fixed aerosol climatology in our future projections (stationary forcing over 2005-2100 in version 3.10 and over the entire period in version 3.14), that is limited to the aerosol direct effect (indirect effects are neglected). This prevents the possibility of investigating the local cooling related to particle pollution that is mainly active at the bottom of the valley (Napoli et al., 2022) and that is currently decreasing in Europe with a significant impact on surface temperature (Philipona, 2012 ; Tudoroiu et al., 2016 ; Nabat et al., 2025). (ii) The model also uses a stationary land surface cover which excludes the possible effect of the migration of the tree line on EDW. These two aspects should be investigated in future work.

600

605

Further research could also investigate other processes acting as feedback on EDW. An increase in humidity (i.e. atmospheric moisture) entails an increase in the downward longwave radiation, and the Planck feedback entails an increase in the upward longwave radiation. Moreover, seasonal contrasts may be reinforced due to these processes : in winter, humidity is higher than in summer and temperature is lower, potentially strengthening one process over the other in winter and switching in summer. These two effects are implicitly resolved in our modelling framework, but a detailed investigation should be done to properly quantify their

610



615 impact. We found the impact of atmospheric moisture challenging to assess in this study, for
two reasons : (i) it is hard to disentangle its trend with the temperature trend and to know which
cause came first, as higher temperature often leads to higher humidity which in turn impacts
warming, in a feedback loop ; and (ii) it is not clear whether atmospheric moisture is expected
620 to have an increasing or decreasing impact on EDW. Several studies argue that it has an
increasing impact (Pepin et al., 2015 ; Ruckstuhl et al., 2007 and Rangwala et al., 2010), but
the effect on EDW has been found to be the opposite in Byrne et al. (2024) (opposing EDW
instead of increasing it) and to have no effect in Minder et al. (2018).

Convection could explain the enhanced warming at 500hPa (upper part of the hook shape
625 seen in the free atmosphere trends) as more humidity is brought to high elevations and
condenses, releasing heat (as seen in the tropics in Romps, 2011 and Keil et al., 2023 ; in the
tropics and to a lesser extent at midlatitudes in Vallis et al., 2015 ; in the Tibetan Plateau in Wei
et al., 2025). The Planck feedback could also explain this signal, since it is expected to induce
positive EDW (Pepin et al., 2015) which would favor higher warming at high elevations.
630 Explaining the slightly enhanced warming at 925hPa (lower part of the hook shape in the free
atmosphere trends, and to some degree near the surface) is more challenging. As mentioned
in the previous paragraph, atmospheric moisture has a negative EDW signal (favoring low
elevations) according to Byrne et al. (2024) which could explain this signal, however other
studies also cited in the previous paragraph predict a positive EDW signal from atmospheric
635 moisture. Another possible explanation could be the enhanced warming during inversion layer
events of the lowest atmospheric layer (Ohmura, 2012).

It is interesting to note that the hook shape can also be seen in the winter months in Minder et
al. (2018) in the Rocky Mountains for the free troposphere EDW, although they found no
impact of atmospheric moisture on EDW in general. Further investigation would be needed to
640 fully characterize the signals driving this hook shape warming in the troposphere.

Overall, we highlight a decoupling between the free atmosphere and the elevated surface
areas, with a strong EDW along the slopes induced by surface feedbacks that is not occurring
in the free atmosphere.

645

Appendices

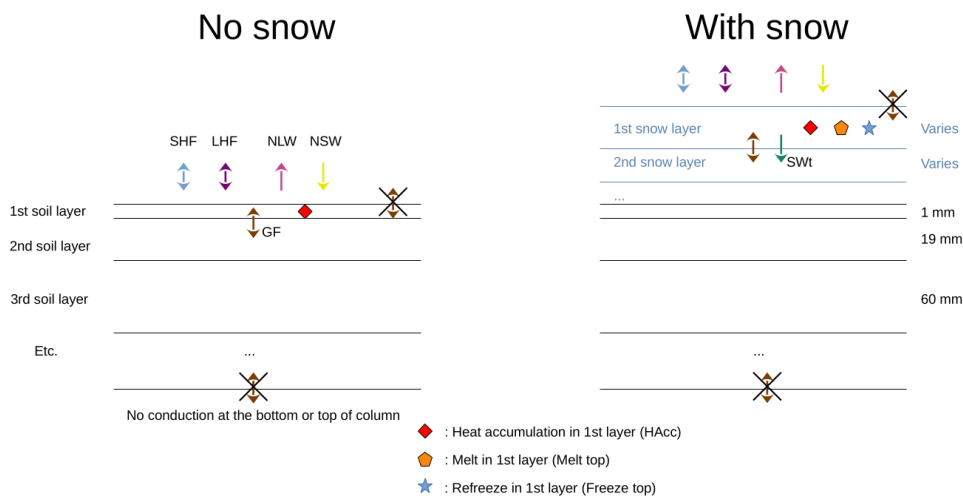
A - MAR output data and surface energy balance

The outputs of the version 3.10 experiments are available at different height and pressure
levels (2, 10, 50, 100m and 925, 850, 800, 700, 600, 500, 200 hPa for the daily mean
650 temperature), and the first 3 sigma levels (for Tmax and Tmin).
The version 3.14 experiment is available at 2, 10, 100m and 850, 700, 600, 500, 200 hPa for
the daily mean temperature, and the first 2 sigma levels for Tmax and Tmin. Its output also
features the melt/freeze top, GF, HAcc, and SWt variables unlike version 3.10.

655 Figure A1 describes the surface energy balance in the soil and snow routine in MAR. It is
computed for the top layer, which is 1mm thick when there is no snow on the ground, and of



variable thickness when there is snow (depending on the amount of recent snowfall and the evolution of the snowpack).



660

Figure A1 : Surface energy balance variables in MAR soil and snow routine, with and without snow present on the ground. MAR has a total of 6 soil layers and up to 20 snow layers.

B - Comparison of MAR simulations to gridded observation datasets

665 In this section, we briefly compare the MAR simulations at 7km resolution used in our study to gridded observational datasets based on station interpolation and gap-filled satellite observations.

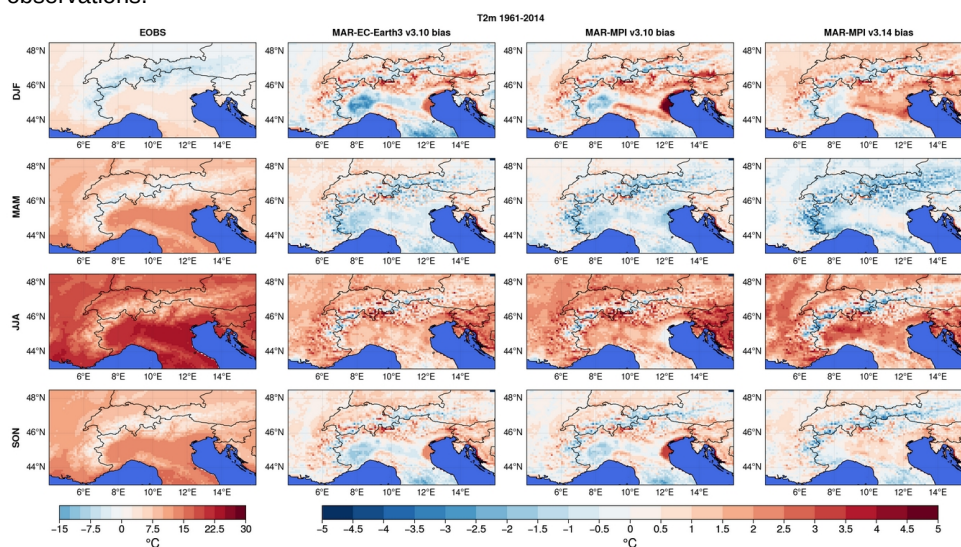


Figure B1 : First column : Mean daily temperature at 2m (T2m) for each season averaged



20

670 over 1961-2014 for E-OBS. Next three columns : Difference between MAR simulations
(forced by EC-Earth3 and MPI-ESM1-2-HR using version 3.10 of MAR, and by MPI-ESM1-2-
HR using version 3.14 of MAR for the 2nd, 3rd and 4th columns respectively) and E-OBS
over the same period.

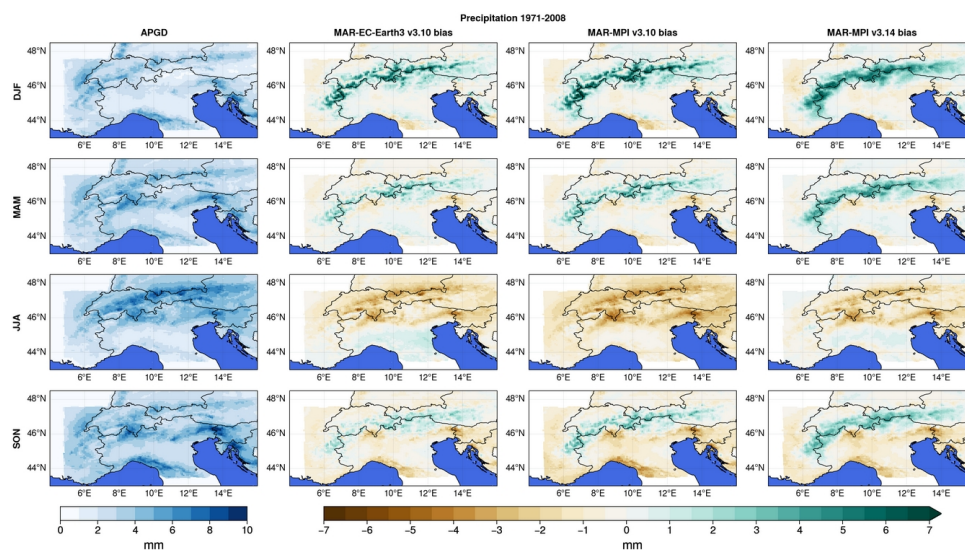
675 Figure B1 shows the temperature bias for the historical period of our MAR GCM-driven
simulations compared to E-OBS.

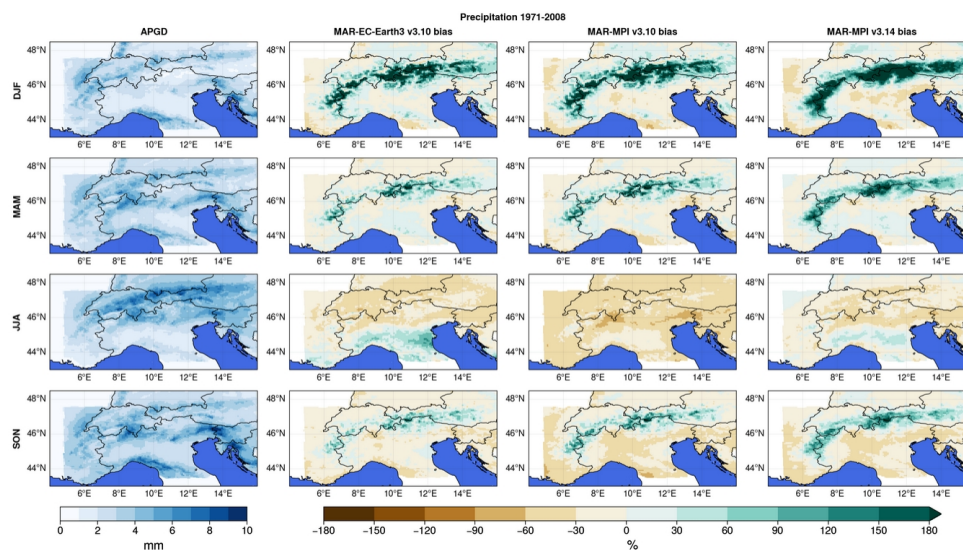
E-OBS is a high resolution ($0.1^\circ \times 0.1^\circ$) gridded dataset over Europe based on daily station
time series from the European Climate Assessment & Dataset (ECA&D). It uses an
interpolation algorithm to produce an ensemble of reconstructions (Cornes et al., 2018). We
use here the ensemble mean for daily mean air temperature in the version 29 of the dataset.

680

With some exceptions, all three simulations have similar biases compared to E-OBS. A cold
bias at high altitudes of about 3°C stands out for all simulations and all seasons. In summer,
the lowlands present a warm bias of around 2°C for MAR-EC-Earth3 and 3°C for both
MAR-MPI simulations, reaching 4°C in some locations. Autumn and winter show contrasted
biases ranging generally from -2 to $+2^\circ\text{C}$ for the former and -3 to $+3^\circ\text{C}$ for the latter. In
685 spring, all simulations show a cold bias to the south of the Alps but show different signs to
the north - these also range generally from -2 to $+2^\circ\text{C}$.

690





695 Figure B2 : Same as Fig. B1 but for daily precipitation, using APGD. Difference is given in mm at the top and in percent at the bottom relative to APGD.

700 Figure B2 shows the daily precipitation bias for the period 1971-2008 of the MAR simulations compared to the Alpine precipitation grid dataset (APGD). APGD is a pan-Alpine grid dataset based on rain-gauge data using an interpolation method that integrates climatological precipitation-topography relationships (Isotta et al., 2014).

All three simulations have once again similar biases. There is a positive bias in the Alps, especially at high elevations, in winter, spring and autumn. The bias is highest in winter with values reaching up to 7mm and over 180 % relative to APGD.

705 In summer, the bias becomes negative in the Alps with values reaching 5mm for some locations, or over 60 % relative to APGD.

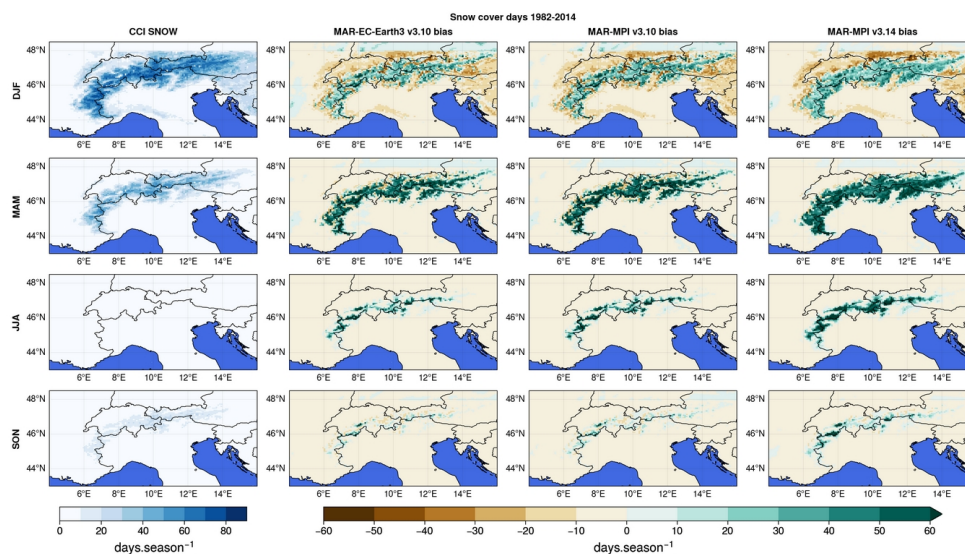


Figure B3 : Same as Fig. A1 but for the number of days per season with snow on the ground, using SNOW-CCI. A grid point in MAR is considered to have snow if it has >50 mmWe of snow.
 710

Figure B3 shows the bias for the number of days with snow on the ground per season for the MAR simulations compared to the SNOW-CCI dataset.

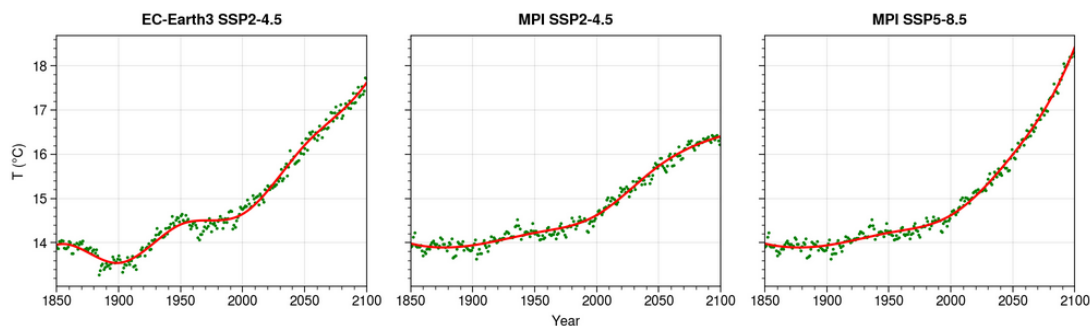
SNOW-CCI is a satellite observation product that has been gap-filled, using a linear interpolation of the data for windows of missing data with a maximum duration of 10 days (see Lalande et al., 2023). A second algorithm is used to count the number of snow days for each grid cell. A grid cell is considered to have snow if it is covered at least 50 % in snow. To account for the remaining gaps not filled by the abovementioned interpolation, the available data is extrapolated at the monthly timescale (Derksen et al., 2025) - for X snow covered days among Y available daily data per month, we have SCD the snow cover duration :
 715
 720 $SCD = X/Y * [\text{number of days in the month}]$

The extrapolation is performed only if there are at least 15 days of available data in the month.

The three simulations again show similar biases : there is a positive bias at high elevations in summer and autumn up to 60 days/season, and no bias at low elevations. The positive bias extends to the entire Alps in winter and spring, with winter having additionally a negative bias at low elevations surrounding the Alps of about 20-30 days/season.
 725



C - GCM warming splines



730 Figure C1 : Spline fit (red) of yearly global warming at 2m average series (green) in the forcing GCM simulations. We used a 3rd degree B-spline with 4 knots.

Figure C1 shows the smoothed warming in the GCMs used to force the MAR simulations used in this study. All three start at 14 °C global temperature and rise (from least to most) by 735 2.4 °C for MPI-ESM1-2-HR using the SSP2-4.5 scenario, 3.6 °C for EC-Earth3 with the same scenario, and 4.5 °C for MPI-ESM1-2-HR using the SSP5-8.5 scenario by the end of the 21st century.

Using these three experiments to force MAR allows us to have a spread in the forcings at the simulations' boundaries.

740 D - Elevation of maximum trend

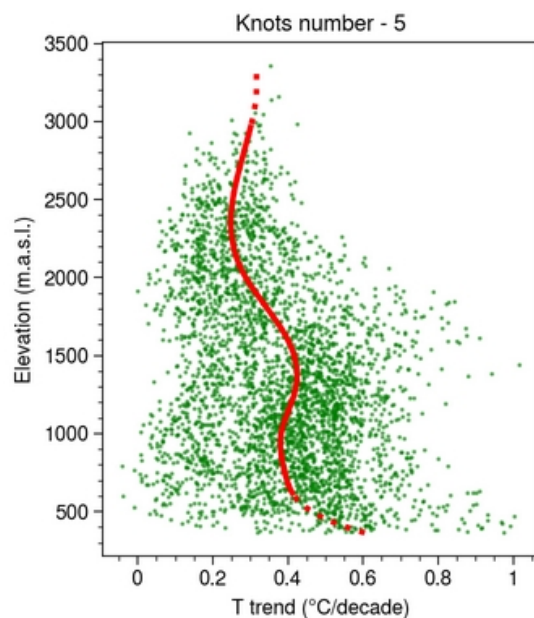




Figure D1 : Warming in the Alps during a given 50-year window, with a fit using a 3rd degree B-spline using 5 knots (red). Green dots are the warming for individual grid points. Dashed line : full spline. Full line : we cut off 10 % of the lower altitudes and 0.3 % of the highest to ensure that we target the local maximum around 1500 meters.

Figure D1 shows the method used to identify the elevation of the maximum warming, by smoothing the data with a spline.

Code and data availability

All scripts to produce the figures are available at https://github.com/lan-CD/PhD/tree/master/Article_EDW. The Python environment used is also included.

The MAR simulations are available on Zenodo repositories.
Version 3.10 : Beaumet et al., 2022a (<https://doi.org/10.5281/zenodo.5834221>), Beaumet et al., 2022b (<https://doi.org/10.5281/zenodo.5834376>), Beaumet et al., 2022c (<https://doi.org/10.5281/zenodo.5838345>)
Version 3.14 : Castellanos et al., 2025a (<https://doi.org/10.5281/zenodo.17534365>), Castellanos et al., 2025b (<https://doi.org/10.5281/zenodo.17569252>)

The E-OBS temperature dataset was downloaded from Copernicus servers. The APGD precipitation dataset (DOI : 10.18751/Climate/Griddata/APGD/1.0) was also retrieved from Copernicus servers. The Snow CCI dataset was downloaded at <https://doi.org/10.5285/3f034f4a08854eb59d58e1fa92d207b6> (Naegeli et al., 2022).

Author contributions

MM and JB¹ produced the MAR version 3.10 simulations, IC produced the MAR version 3.14 simulation. HG and XF developed MAR and provided helpful discussion and information on the model. EM-C provided the EC-Earth3 forcing files. MM and JB² contributed to the design and the direction of the study. IC produced the figures and wrote the article, and all authors contributed with suggested changes and helpful comments.

¹Julien Beaumet

²Juliette Blanchet

Competing interests

The authors declare that they have no conflict of interest.



25

Acknowledgements

The authors thank Nathan Philippot and Mickaël Lalande for their help in writing code. We also thank Charles Amory and Cécile Agosta for their help with the model MAR. To access
785 the general circulation model data, this study also benefited from the IPSL mesocenter
ESPRI facility which is supported by CNRS, UPMC, Labex L-IPSL, CNES and Ecole
Polytechnique. All (or most of) the computations presented in this paper were performed
using the GRICAD infrastructure (<https://gricad.univ-grenoble-alpes.fr>), which is supported
by Grenoble research communities.

790 Financial support

This research was funded by the Agence Nationale de la Recherche (ANR) through the
ClimAir project (ANR-22-CE03-0004).

References

- Agosta, C., Amory, C., Kittel, C., Orsi, A., Favier, V., Gallée, H., van den Broeke, M. R.,
795 Lenaerts, J. T. M., van Wessem, J. M., van de Berg, W. J., and Fettweis, X.: Estimation of
the Antarctic surface mass balance using the regional climate model MAR (1979–2015) and
identification of dominant processes, *The Cryosphere*, 13, 281–296,
<https://doi.org/10.5194/tc-13-281-2019>, 2019.
- Amory, C., Kittel, C., Le Toumelin, L., Agosta, C., Delhasse, A., Favier, V., and Fettweis, X.:
800 Performance of MAR (v3.11) in simulating the drifting-snow climate and surface mass
balance of Adélie Land, East Antarctica, *Geoscientific Model Development*, 14, 3487–3510,
<https://doi.org/10.5194/gmd-14-3487-2021>, 2021.
- Bacer, S., Beaumet, J., Ménégot, M., Gallée, H., Le Bouëdec, E., and Staquet, C.: Impact of
805 climate change on persistent cold-air pools in an alpine valley during the 21st century,
Weather and Climate Dynamics, 5, 211–229, <https://doi.org/10.5194/wcd-5-211-2024>, 2024.
- Barrios, G. C.: San Rafael Glacier and Northern Patagonia Icefield surface mass balance
estimation from different approaches, phdthesis, Université Grenoble Alpes, 2018.
810
- Beaumet, J., Ménégot, M., Morin, S., Gallée, H., Fettweis, X., Six, D., Vincent, C., Wilhelm,
B., and Anquetin, S.: Twentieth century temperature and snow cover changes in the French
Alps, *Reg Environ Change*, 21, 114, <https://doi.org/10.1007/s10113-021-01830-x>, 2021.
- 815 Beaumet, J., Menegot, M., Gallée, H., and Chamarro, E. M.: MAR-EC-Earth3 HIST (1961-
2014) and SSP245 European Alps (2015-2100), <https://doi.org/10.5281/zenodo.5838345>,
2022a.



820 Beaumet, J., Menegoz, M., and Gallée, H.: MAR-MPI-ESM1-2-HR SSP585 European Alps
(2015-2100), <https://doi.org/10.5281/zenodo.5834376>, 2022b.

Beaumet, J., Menegoz, M., and Gallée, H.: MAR-MPI-ESM1-2-HR HIST (1961-2014) and
SSP245 European Alps (2015-2100), <https://doi.org/10.5281/zenodo.5834221>, 2022c

825 Bozzo, A., Benedetti, A., Flemming, J., Kipling, Z., and Rémy, S.: An aerosol climatology for
global models based on the tropospheric aerosol scheme in the Integrated Forecasting
System of ECMWF, Geoscientific Model Development, 13, 1007–1034,
<https://doi.org/10.5194/gmd-13-1007-2020>, 2020.

830 Brun, E., David, P., Sudul, M., and Brunot, G.: A numerical model to simulate snow-cover
stratigraphy for operational avalanche forecasting, Journal of Glaciology, 38, 13–22,
<https://doi.org/10.3189/S0022143000009552>, 1992.

835 Byrne, M. P., Boos, W. R., and Hu, S.: Elevation-dependent warming: observations, models,
and energetic mechanisms, Weather and Climate Dynamics, 5, 763–777,
<https://doi.org/10.5194/wcd-5-763-2024>, 2024.

840 Castellanos, I., Ménéguez, M., and Gallée, H.: MARv3.14-MPI-ESM1-2-HR HIST European
Alps (1961-2014), <https://doi.org/10.5281/zenodo.17569252>, 2025a.

Castellanos, I., Ménéguez, M., and Gallée, H.: MARv3.14-MPI-ESM1-2-HR SSP585
European Alps (2015-2100), <https://doi.org/10.5281/zenodo.17534365>, 2025b.

845 Chagnaud, G., Gallée, H., Lebel, T., Panthou, G., and Vischel, T.: A Boundary Forcing
Sensitivity Analysis of the West African Monsoon Simulated by the Modèle Atmosphérique
Régional, Atmosphere, 11, 191, <https://doi.org/10.3390/atmos11020191>, 2020.

850 Colombo, N., Guyennon, N., Valt, M., Salerno, F., Godone, D., Cianfarra, P., Freppaz, M.,
Maugeri, M., Manara, V., Acquafredda, F., Petrangeli, A. B., and Romano, E.: Unprecedented
snow-drought conditions in the Italian Alps during the early 2020s, Environ. Res. Lett., 18,
074014, <https://doi.org/10.1088/1748-9326/acdb88>, 2023.

855 Cornes, R. C., van der Schrier, G., van den Besselaar, E. J. M., and Jones, P. D.: An
Ensemble Version of the E-OBS Temperature and Precipitation Data Sets, Journal of
Geophysical Research: Atmospheres, 123, 9391–9409,
<https://doi.org/10.1029/2017JD028200>, 2018.



- Delhasse, A., Kittel, C., Amory, C., Hofer, S., van As, D., S. Fausto, R., and Fettweis, X.:
Brief communication: Evaluation of the near-surface climate in ERA5 over the Greenland Ice
860 Sheet, *The Cryosphere*, 14, 957–965, <https://doi.org/10.5194/tc-14-957-2020>, 2020.
- Derksen, C., Essery, R., Gustafsson, D., Menegoz, M., Krinner, G., and de Rosnay, P.:
Snow CCI Climate Assessment Report, 2025
- 865 Dimri, A. P., Choudhary, A., and Kumar, D.: Elevation Dependent Warming over Indian
Himalayan Region, 141–156, https://doi.org/10.1007/978-3-030-29684-1_9, 2020.
- Dimri, A. P., Palazzi, E., and Daloz, A. S.: Elevation dependent precipitation and
temperature changes over Indian Himalayan region, *Clim Dyn*, 59, 1–21,
870 <https://doi.org/10.1007/s00382-021-06113-z>, 2022.
- Eyring, V., Bony, S., Meehl, G. A., Senior, C. A., Stevens, B., Stouffer, R. J., and Taylor, K.
E.: Overview of the Coupled Model Intercomparison Project Phase 6 (CMIP6) experimental
design and organization, *Geoscientific Model Development*, 9, 1937–1958,
875 <https://doi.org/10.5194/gmd-9-1937-2016>, 2016.
- Fettweis, X., Box, J. E., Agosta, C., Amory, C., Kittel, C., Lang, C., van As, D., Machguth, H.,
and Gallée, H.: Reconstructions of the 1900–2015 Greenland ice sheet surface mass
balance using the regional climate MAR model, *The Cryosphere*, 11, 1015–1033,
880 <https://doi.org/10.5194/tc-11-1015-2017>, 2017.
- Fettweis, X., B, A., P.m, D., Ghilain, N., P, P., and C, W.: Évolution actuelle (1960-2021) de
l'enneigement dans les Vosges à l'aide du modèle régional du climat MAR, *Bulletin de la
885 Société Géographique de Liège*, 80, <https://doi.org/10.25518/0770-7576.7049>, 2023.
- Gallée, H. and Schayes, G.: Development of a Three-Dimensional Meso- γ Primitive
Equation Model: Katabatic Winds Simulation in the Area of Terra Nova Bay, Antarctica,
Monthly Weather Review, 122, 671–685, [https://doi.org/10.1175/1520-
0493\(1994\)122<0671:DOATDM>2.0.CO;2](https://doi.org/10.1175/1520-0493(1994)122<0671:DOATDM>2.0.CO;2), 1994.
890
- Gallée, H., Peyaud, V., and Goodwin, I.: Simulation of the net snow accumulation along the
Wilkes Land transect, Antarctica, with a regional climate model, *Annals of Glaciology*, 41,
17–22, <https://doi.org/10.3189/172756405781813230>, 2005.
- 895 Glaude, Q., Noel, B., Olesen, M., Van den Broeke, M., van de Berg, W. J., Mottram, R.,
Hansen, N., Delhasse, A., Amory, C., Kittel, C., Goelzer, H., and Fettweis, X.: A Factor Two



- Difference in 21st-Century Greenland Ice Sheet Surface Mass Balance Projections From Three Regional Climate Models Under a Strong Warming Scenario (SSP5-8.5), *Geophysical Research Letters*, 51, e2024GL111902, <https://doi.org/10.1029/2024GL111902>, 2024.
- 900
- Gobiet, A., Kotlarski, S., Beniston, M., Heinrich, G., Rajczak, J., and Stoffel, M.: 21st century climate change in the European Alps—A review, *Science of The Total Environment*, 493, 1138–1151, <https://doi.org/10.1016/j.scitotenv.2013.07.050>, 2014.
- 905
- Grailet, J.-F.: Inclusion of a new radiative transfer scheme in the MAR model and validation on Belgium, *BSGLg*, <https://doi.org/10.25518/0770-7576.7031>, 2023.
- Hogan, R. J. and Bozzo, A.: A Flexible and Efficient Radiation Scheme for the ECMWF Model, *Journal of Advances in Modeling Earth Systems*, 10, 1990–2008,
- 910 <https://doi.org/10.1029/2018MS001364>, 2018.
- Isotta, F. A., Frei, C., Weilguni, V., Perčec Tadić, M., Lassègues, P., Rudolf, B., Pavan, V., Cacciamani, C., Antolini, G., Ratto, S. M., Munari, M., Micheletti, S., Bonati, V., Lussana, C., Ronchi, C., Panettieri, E., Marigo, G., and Vertačnik, G.: The climate of daily precipitation in the Alps: development and analysis of a high-resolution grid dataset from pan-Alpine rain-gauge data, *International Journal of Climatology*, 34, 1657–1675,
- 915 <https://doi.org/10.1002/joc.3794>, 2014.
- Keil, P., Schmidt, H., Stevens, B., Byrne, M. P., Segura, H., and Putrasahan, D.: Tropical tropospheric warming pattern explained by shifts in convective heating in the Matsuno–Gill model, *Quarterly Journal of the Royal Meteorological Society*, 149, 2678–2695,
- 920 <https://doi.org/10.1002/qj.4526>, 2023.
- Kotlarski, S., Bosshard, T., Lüthi, D., Pall, P., and Schär, C.: Elevation gradients of European climate change in the regional climate model COSMO-CLM, *Climatic Change*, 112, 189–215, <https://doi.org/10.1007/s10584-011-0195-5>, 2012.
- 925
- Kotlarski, S., Lüthi, D., and Schär, C.: The elevation dependency of 21st century European climate change: an RCM ensemble perspective, *International Journal of Climatology*, 35, 3902–3920, <https://doi.org/10.1002/joc.4254>, 2015.
- 930
- Kotlarski, S., Szabó, P., Herrera, S., Rätty, O., Keuler, K., Soares, P. M., Cardoso, R. M., Bosshard, T., Pagé, C., Boberg, F., Gutiérrez, J. M., Isotta, F. A., Jaczewski, A., Kreienkamp, F., Liniger, M. A., Lussana, C., and Pianko-Kluczyńska, K.: Observational



- 935 uncertainty and regional climate model evaluation: A pan-European perspective,
International Journal of Climatology, 39, 3730–3749, <https://doi.org/10.1002/joc.5249>, 2019.
- Kotlarski, S., Gobiet, A., Morin, S., Olefs, M., Rajczak, J., and Samacoïts, R.: 21st Century
alpine climate change, *Clim Dyn*, 60, 65–86, <https://doi.org/10.1007/s00382-022-06303-3>,
940 2023.
- Kouassi, A., Assamoi, P., Bigot, S., Diawara, A., Schayes, G., Yoroba, F., and Kouassi, B.:
Étude du climat Ouest-Africain à l'aide du modèle atmosphérique régional M.A.R.,
Climatologie, 7, 39–55, <https://doi.org/10.4267/climatologie.445>, 2010.
945
- Kuhn, M. and Olefs, M.: Elevation-Dependent Climate Change in the European Alps, in:
Oxford Research Encyclopedia of Climate Science,
<https://doi.org/10.1093/acrefore/9780190228620.013.762>, 2020.
- 950 Lalande, M., Ménégoz, M., Krinner, G., Otlé, C., and Cheruy, F.: Improving climate model
skill over High Mountain Asia by adapting snow cover parameterization to complex-
topography areas, *The Cryosphere*, 17, 5095–5130, [https://doi.org/10.5194/tc-17-5095-
2023](https://doi.org/10.5194/tc-17-5095-2023), 2023.
- 955 Li, B., Chen, Y., and Shi, X.: Does elevation dependent warming exist in high mountain
Asia?, *Environ. Res. Lett.*, 15, 024012, <https://doi.org/10.1088/1748-9326/ab6d7f>, 2020.
- Lüthi, S., Ban, N., Kotlarski, S., Steger, C. R., Jonas, T., and Schär, C.: Projections of Alpine
Snow-Cover in a High-Resolution Climate Simulation, *Atmosphere*, 10, 463,
960 <https://doi.org/10.3390/atmos10080463>, 2019.
- Matiu, M., Petitta, M., Notarnicola, C., and Zebisch, M.: Evaluating Snow in EURO-CORDEX
Regional Climate Models with Observations for the European Alps: Biases and Their
Relationship to Orography, Temperature, and Precipitation Mismatches, *Atmosphere*, 11,
965 46, <https://doi.org/10.3390/atmos11010046>, 2020.
- Matiu, M., Napoli, A., Kotlarski, S., Zardi, D., Bellin, A., and Majone, B.: Elevation-dependent
biases of raw and bias-adjusted EURO-CORDEX regional climate models in the European
Alps, *Clim Dyn*, 62, 9013–9030, <https://doi.org/10.1007/s00382-024-07376-y>, 2024.
970
- Ménégoz, M., Gallée, H., and Jacobi, H. W.: Precipitation and snow cover in the Himalaya:
from reanalysis to regional climate simulations, *Hydrology and Earth System Sciences*, 17,
3921–3936, <https://doi.org/10.5194/hess-17-3921-2013>, 2013.



30

- 975 Ménégoz, M., Valla, E., Jourdain, N. C., Blanchet, J., Beaumet, J., Wilhelm, B., Gallée, H., Fettweis, X., Morin, S., and Anquetin, S.: Contrasting seasonal changes in total and intense precipitation in the European Alps from 1903 to 2010, *Hydrology and Earth System Sciences*, 24, 5355–5377, <https://doi.org/10.5194/hess-24-5355-2020>, 2020.
- 980 Minder, J. R., Letcher, T. W., and Liu, C.: The Character and Causes of Elevation-Dependent Warming in High-Resolution Simulations of Rocky Mountain Climate Change, *Journal of Climate*, 31, 2093–2113, <https://doi.org/10.1175/JCLI-D-17-0321.1>, 2018.
- Morcrette, J.-J.: Radiation and cloud radiative properties in the European Centre for Medium
985 Range Weather Forecasts forecasting system, *Journal of Geophysical Research: Atmospheres*, 96, 9121–9132, <https://doi.org/10.1029/89JD01597>, 1991.
- Morcrette, J.-J.: The Surface Downward Longwave Radiation in the ECMWF Forecast
990 System, *Journal of Climate*, 15, 1875–1892, [https://doi.org/10.1175/1520-0442\(2002\)015<1875:TSDLRI>2.0.CO;2](https://doi.org/10.1175/1520-0442(2002)015<1875:TSDLRI>2.0.CO;2), 2002.
- Nabat, P., Somot, S., Boé, J., Corre, L., Katragkou, E., Li, S., Mallet, M., van Meijgaard, E., Pavlidis, V., Pietikäinen, J.-P., Sørland, S., and Solomon, F.: Multi-Model Assessment of the
995 Role of Anthropogenic Aerosols in Summertime Climate Change in Europe, *Geophysical Research Letters*, 52, e2024GL112474, <https://doi.org/10.1029/2024GL112474>, 2025.
- Naegeli, K., Neuhaus, C., Salberg, A.-B., Schwaizer, G., Weber, H., Wiesmann, A., Wunderle, S., and Nagler, T.: ESA Snow Climate Change Initiative (Snow_cci): Daily global
1000 Snow Cover Fraction - snow on ground (SCFG) from AVHRR (1982 - 2018), version 2.0, <https://doi.org/10.5285/3F034F4A08854EB59D58E1FA92D207B6>, 2022.
- Napoli, A., Desbiolles, F., Parodi, A., and Pasquero, C.: Aerosol indirect effects in complex-
orography areas: a numerical study over the Great Alpine Region, *Atmospheric Chemistry and Physics*, 22, 3901–3909, <https://doi.org/10.5194/acp-22-3901-2022>, 2022.
1005
- Napoli, A., Parodi, A., von Hardenberg, J., and Pasquero, C.: Altitudinal dependence of
projected changes in occurrence of extreme events in the Great Alpine Region, *International Journal of Climatology*, 43, 5813–5829, <https://doi.org/10.1002/joc.8222>, 2023.
- 1010 Ohmura, A.: Enhanced temperature variability in high-altitude climate change, *Theoretical and Applied Climatology*, 110, <https://doi.org/10.1007/s00704-012-0687-x>, 2012.



- O'Neill, B. C., Tebaldi, C., van Vuuren, D. P., Eyring, V., Friedlingstein, P., Hurtt, G., Knutti, R., Kriegler, E., Lamarque, J.-F., Lowe, J., Meehl, G. A., Moss, R., Riahi, K., and Sanderson, B. M.: The Scenario Model Intercomparison Project (ScenarioMIP) for CMIP6, *Geoscientific Model Development*, 9, 3461–3482, <https://doi.org/10.5194/gmd-9-3461-2016>, 2016.
- Palazzi, E., Filippi, L., and von Hardenberg, J.: Insights into elevation-dependent warming in the Tibetan Plateau-Himalayas from CMIP5 model simulations, *Clim Dyn*, 48, 3991–4008, <https://doi.org/10.1007/s00382-016-3316-z>, 2017.
- Palazzi, E., Mortarini, L., Terzago, S., and von Hardenberg, J.: Elevation-dependent warming in global climate model simulations at high spatial resolution, *Clim Dyn*, 52, 2685–2702, <https://doi.org/10.1007/s00382-018-4287-z>, 2019.
- Pepin, N., Bradley, R. S., Diaz, H. F., Baraer, M., Caceres, E. B., Forsythe, N., Fowler, H., Greenwood, G., Hashmi, M. Z., Liu, X. D., Miller, J. R., Ning, L., Ohmura, A., Palazzi, E., Rangwala, I., Schöner, W., Severskiy, I., Shahgedanova, M., Wang, M. B., Williamson, S. N., Yang, D. Q., and Mountain Research Initiative EDW Working Group: Elevation-dependent warming in mountain regions of the world, *Nature Clim Change*, 5, 424–430, <https://doi.org/10.1038/nclimate2563>, 2015.
- Pepin, N., Apple, M., Knowles, J., Terzago, S., Arnone, E., Hänchen, L., Napoli, A., Potter, E., Steiner, J., Williamson, S. N., Ahrens, B., Dhar, T., Dimri, A. P., Palazzi, E., Rameshan, A., Salzmann, N., Shahgedanova, M., Vidal Jr, J. de D., and Zardi, D.: Elevation-dependent climate change in mountain environments, *Nat Rev Earth Environ*, 6, 772–788, <https://doi.org/10.1038/s43017-025-00740-4>, 2025.
- Pepin, N. C. and Seidel, D. J.: A global comparison of surface and free-air temperatures at high elevations, *Journal of Geophysical Research: Atmospheres*, 110, <https://doi.org/10.1029/2004JD005047>, 2005.
- Pepin, N. C., Arnone, E., Gobiet, A., Haslinger, K., Kotlarski, S., Notarnicola, C., Palazzi, E., Seibert, P., Serafin, S., Schöner, W., Terzago, S., Thornton, J. M., Vuille, M., and Adler, C.: Climate Changes and Their Elevational Patterns in the Mountains of the World, *Reviews of Geophysics*, 60, e2020RG000730, <https://doi.org/10.1029/2020RG000730>, 2022.
- Philipona, R.: Greenhouse warming and solar brightening in and around the Alps, *International Journal of Climatology*, 33, 1530–1537, <https://doi.org/10.1002/joc.3531>, 2013.



- Prein, A. F. and Gobiet, A.: Impacts of uncertainties in European gridded precipitation observations on regional climate analysis, *International Journal of Climatology*, 37, 305–327, <https://doi.org/10.1002/joc.4706>, 2017.
- 1055 Rahbek, C., Borregaard, M. K., Colwell, R. K., Dalsgaard, B., Holt, B. G., Morueta-Holme, N., Nogues-Bravo, D., Whittaker, R. J., and Fjeldså, J.: Humboldt's enigma: What causes global patterns of mountain biodiversity?, *Science*, 365, 1108–1113, <https://doi.org/10.1126/science.aax0149>, 2019.
- 1060 Rangwala, I., Miller, J. R., Russell, G. L., and Xu, M.: Using a global climate model to evaluate the influences of water vapor, snow cover and atmospheric aerosol on warming in the Tibetan Plateau during the twenty-first century, *Clim Dyn*, 34, 859–872, <https://doi.org/10.1007/s00382-009-0564-1>, 2010.
- 1065 Romps, D. M.: Response of Tropical Precipitation to Global Warming, *Journal of the Atmospheric Sciences*, 68, 123–138, <https://doi.org/10.1175/2010JAS3542.1>, 2011.
- Rottler, E., Kormann, C., Francke, T., and Bronstert, A.: Elevation-dependent warming in the Swiss Alps 1981–2017: Features, forcings and feedbacks, *International Journal of*
- 1070 *Climatology*, 39, 2556–2568, <https://doi.org/10.1002/joc.5970>, 2019.
- Ruckstuhl, C., Philipona, R., Morland, J., and Ohmura, A.: Observed relationship between surface specific humidity, integrated water vapor, and longwave downward radiation at different altitudes, *J. Geophys. Res.*, 112, 2006JD007850,
- 1075 <https://doi.org/10.1029/2006JD007850>, 2007.
- Sandu, I., van Niekerk, A., Shepherd, T. G., Vosper, S. B., Zadra, A., Bacmeister, J., Beljaars, A., Brown, A. R., Dörnbrack, A., McFarlane, N., Pithan, F., and Svensson, G.: Impacts of orography on large-scale atmospheric circulation, *npj Clim Atmos Sci*, 2, 10,
- 1080 <https://doi.org/10.1038/s41612-019-0065-9>, 2019.
- Sobolowski, S., Somot, S., Fernandez, J., Evin, G., Brands, S., Maraun, D., Kotlarski, S., Jury, M., Benestad, R. E., Teichmann, C., Christensen, O. B., Bülow, K., Buonomo, E., Katragkou, E., Steger, C., Sørland, S., Nikulin, G., McSweeney, C., Dobler, A., Palmer, T.,
- 1085 Wilcke, R., Boé, J., Brunner, L., Ribes, A., Qasmi, S., Nabat, P., Sevault, F., and Oudar, T.: GCM Selection and Ensemble Design: Best Practices and Recommendations from the EURO-CORDEX Community, *Bulletin of the American Meteorological Society*, 106, E1834–E1850, <https://doi.org/10.1175/BAMS-D-23-0189.1>, 2025.



- 1090 Terzago, S., von Hardenberg, J., Palazzi, E., and Provenzale, A.: Snow water equivalent in the Alps as seen by gridded data sets, CMIP5 and CORDEX climate models, *The Cryosphere*, 11, 1625–1645, <https://doi.org/10.5194/tc-11-1625-2017>, 2017.
- Thornton, J. M., Palazzi, E., Pepin, N. C., Cristofanelli, P., Essery, R., Kotlarski, S., Giuliani, G., Guigoz, Y., Kulonen, A., Pritchard, D., Li, X., Fowler, H. J., Randin, C. F., Shahgedanova, M., Steinbacher, M., Zebisch, M., and Adler, C.: Toward a definition of Essential Mountain Climate Variables, *One Earth*, 4, 805–827, <https://doi.org/10.1016/j.oneear.2021.05.005>, 2021.
- 1095
- 1100 Toledo, O., Palazzi, E., Cely Toro, I. M., and Mortarini, L.: Comparison of elevation-dependent warming and its drivers in the tropical and subtropical Andes, *Clim Dyn*, 58, 3057–3074, <https://doi.org/10.1007/s00382-021-06081-4>, 2022.
- Tudoroiu, M., Eccel, E., Gioli, B., Gianelle, D., Schume, H., Genesio, L., and Miglietta, F.: Negative elevation-dependent warming trend in the Eastern Alps, *Environ. Res. Lett.*, 11, 044021, <https://doi.org/10.1088/1748-9326/11/4/044021>, 2016.
- 1105
- Vallis, G. K., Zurita-Gotor, P., Cairns, C., and Kidston, J.: Response of the large-scale structure of the atmosphere to global warming, *Quarterly Journal of the Royal Meteorological Society*, 141, 1479–1501, <https://doi.org/10.1002/qj.2456>, 2015.
- 1110
- Viviroli, D., Kummu, M., Meybeck, M., Kallio, M., and Wada, Y.: Increasing dependence of lowland populations on mountain water resources, *Nat Sustain*, 3, 917–928, <https://doi.org/10.1038/s41893-020-0559-9>, 2020.
- 1115
- Warscher, M., Wagner, S., Marke, T., Laux, P., Smiatek, G., Strasser, U., and Kunstmann, H.: A 5 km Resolution Regional Climate Simulation for Central Europe: Performance in High Mountain Areas and Seasonal, Regional and Elevation-Dependent Variations, *Atmosphere*, 10, 682, <https://doi.org/10.3390/atmos10110682>, 2019.
- 1120
- Wei, Y., Wang, Y., Lu, Z., Huang, Y., and Huang, F.: Upper Troposphere Warming Amplification over the Tibetan Plateau, *Journal of Climate*, 38, 5335–5348, <https://doi.org/10.1175/JCLI-D-24-0567.1>, 2025.